




## Investigation of the role of neutron transfer and fusion hindrance in $^{28}\text{Si} + ^{158}\text{Gd}$ at deep sub-barrier energies

Rinku Prajapat <sup>1</sup>, Moumita Maiti <sup>1,\*</sup>, Rishabh Kumar <sup>1</sup>, Malvika Sagwal,<sup>1</sup> Gonika,<sup>2</sup> Chandra Kumar,<sup>2</sup> Rohan Biswas,<sup>2</sup> J. Gehlot,<sup>2</sup> S. Nath,<sup>2</sup> and N. Madhavan<sup>2</sup>

<sup>1</sup>Department of Physics, Indian Institute of Technology Roorkee, Roorkee-247667, Uttarakhand, India

<sup>2</sup>Nuclear Physics Group, Inter-University Accelerator Centre, New Delhi-110067, India



(Received 21 March 2023; revised 24 April 2023; accepted 14 June 2023; published 29 June 2023)

The challenging task in heavy-ion collisions is unambiguously identifying the true fusion events in the deep sub-barrier region. Considering the primary challenge, we have measured fusion excitation functions for  $^{28}\text{Si} + ^{158}\text{Gd}$  reaction at energies above to deep sub-barrier region to decipher the role of multineutron transfer with positive  $Q$  value and fusion hindrance in an asymmetric system. A comparison has been made with our previous measurement for  $^{30}\text{Si} + ^{156}\text{Gd}$  system where only one transfer channel with  $Q > 0$  exists and populates the same compound nucleus  $^{186}\text{Pt}^*$ . The enhancement in fusion cross sections is observed on a reduced scale in the  $^{28}\text{Si} + ^{158}\text{Gd}$  reaction over  $^{30}\text{Si} + ^{156}\text{Gd}$  system at sub-barrier energies. The measured fusion data and extracted barrier distribution have been analyzed within the framework of coupled-channels (CC) programs, CCFULL and empirical channel coupling. Coupling to rotational excitations in projectile and target along with up to  $2n$  transfer channel with positive  $Q$  value is found to be promising to explain the fusion excitation functions except for the lowest energy point. However, the influence of more than two neutrons transfer is insignificant in  $^{28}\text{Si} + ^{158}\text{Gd}$  system. At the lowest energy ( $\approx 14\%$  down the Coulomb barrier), a deviation from standard CC has been found, which may indicate the threshold for fusion hindrance, but additional lower-energy data are needed to prove this. The experimental threshold energy ( $E_S$ ) for fusion hindrance is in good agreement with the empirical formula, and it is consistent with the observed pattern of  $E_S$  as a function of the entrance channel parameter ( $\zeta$ ) for other nearly symmetric and asymmetric systems.

DOI: [10.1103/PhysRevC.107.064616](https://doi.org/10.1103/PhysRevC.107.064616)

### I. INTRODUCTION

In heavy-ion ( $A \geq 4$ ) collisions, various reaction processes, such as fusion and a few nucleon transfers, play an essential role in understanding the interplay between reaction dynamics and associated structural peculiarities [1,2]. In particular, fusion reactions are governed by the quantum penetration model at below to deep sub-barrier energies where complexity is involved due to the influence of different intrinsic degrees of freedom of fusion participants. However, nucleon transfer reactions are initiated at large internuclear distances where the flow of nucleons between the colliding nuclei occurs in a short interaction time  $10^{-22}$  s. In addition, heavy-ion fusion reactions are greatly influenced by the transfer of nucleons, which is still an ongoing quest for fundamental research even though the effect of collective excitations on fusion reactions is somewhat established [1,3–5].

Intense experimental and theoretical efforts have been made to understand the sub-barrier fusion enhancement in comparison to the one-dimensional barrier penetration model (1D-BPM) in the past few years [1,3–10]. This enhancement was explained by the coupled-channels (CC) effect and static deformations of colliding nuclei which distribute the single

barrier into multidimensional barriers known as “barrier distribution” (BD) [5]. However, the role of the positive  $Q$ -value neutron transfer (PQNT) channels on the sub-barrier fusion cross sections is still somewhat ambiguous and, therefore, an interesting research topic [1,3]. In this direction, the first observation of the PQNT effect on the fusion process was proclaimed by Beckerman *et al.* [11] in  $^{58,64}\text{Ni} + ^{58,64}\text{Ni}$  reactions. Subsequently, a series of experiments revealed a close connection between PQNT and sub-barrier fusion enhancement [12–16]. However, no such correlation due to the PQNT channel on fusion was witnessed in Refs. [7,10,17–19]. Our previous measurement of fusion and quasielastic scattering of  $^{30}\text{Si} + ^{156}\text{Gd}$  [7] also did not reveal any significant enhancement in sub-barrier fusion cross section due to  $2n$  transfer with positive  $Q$  value ( $Q_{2n} = +0.8$  MeV). Theoretically, Stelson *et al.* [20,21] proposed a pragmatic approach to deal with the sequential transfer of neutrons, which could trigger the fusion process at a large internuclear distance. Later, an empirical channel coupling (ECC) model was proposed [22] that could account for the multineutron transfer channels with positive  $Q$  value in CC calculations. The above-mentioned facts suggest that PQNT channels and their correlation with the fusion process are a complex job that is not yet fully understood.

Fusion reactions at deep sub-barrier energies where cross sections exhibit a much steeper fall than the standard CC calculations are also of astrophysical interest [1]. First

\*Corresponding author: moumita.maiti@ph.iit.ac.in

experimental evidence of such unexpected behavior known as “fusion hindrance” was observed by Jiang *et al.* [23] in  $^{60}\text{Ni} + ^{89}\text{Y}$  at extreme sub-barrier energies. Subsequently, a set of experiments were undertaken using closed-shell and open-shell medium- and heavy-mass systems [24–31]. This hindrance in deep sub-barrier fusion cross section is often characterized by astrophysical  $S(E_{c.m.})$  factor and logarithmic slope  $L(E_{c.m.})$  and also leaves an open question about their maxima. Ambiguity in the physical origin of fusion hindrance persists, and a few aspects have been nicely pointed out in a recent review article [1], using Ni+Ni, Si+Si, Ca+Zr, and Ni+Mo systems which consist of positive and/or negative  $Q$  values for transfer channels as well as for fusion process. Moreover, if the systems have a positive fusion  $Q$  value, then there should not be a maximum in  $S(E_{c.m.})$  factor visible [1,3]. On the theoretical front, only a few models, viz. sudden, adiabatic, and a smooth transition between them, have been proposed to explain the fusion hindrance [32–34]. However, it would be worth mentioning that  $^{28}\text{Si} + ^{30}\text{Si}$  [15] is the only experimental study in which fusion hindrance was reported even after considering the PQNT couplings in the CC calculations thus far. The aforementioned facts help to examine the role of the PQNT channels and fusion hindrance in deep sub-barrier fusion cross sections using a soft asymmetric system like  $^{28}\text{Si} + ^{158}\text{Gd}$  owing to the scarcity of experimental data.

In this report, we have measured the fusion excitation functions from above ( $\approx 12\%$ ) to deep below ( $\approx 14\%$ ) the Coulomb barrier energies with the following objectives: (i) to decipher the role of multineutron transfer channels with positive  $Q$  value (up to  $6n$  pickup) in the  $^{28}\text{Si} + ^{158}\text{Gd}$  system and comparison with previously measured data for  $^{30}\text{Si} + ^{156}\text{Gd}$  reaction (with negative  $Q$  values except for  $2n$  pickup channel) as both systems form the same compound nucleus  $^{186}\text{Pt}^*$ , (ii) to investigate the fusion hindrance effect at deep sub-barrier energies and comparison with the previously measured data for  $^{30}\text{Si} + ^{156}\text{Gd}$  reaction, and (iii) systematic comparison on the threshold energy for fusion hindrance using various symmetric and asymmetric reactions.

The structure of this work is as follows: Section II presents the experimental method, data analysis is provided in Sec. III, and results and interpretation of data are discussed in Sec. IV. Finally, Sec. V concludes the work.

## II. EXPERIMENTAL METHOD

The measurement of fusion-evaporation residues for  $^{28}\text{Si} + ^{158}\text{Gd}$  reaction was carried out employing the Heavy Ion Reaction Analyser (HIRA) [35], a mass spectrometer at the 15 UD Pelletron accelerator facility of the Inter-University Accelerator Center (IUAC), New Delhi, India. The experimental setup and procedure were analogous to that used in a previous measurement [7]. However, some of the specific details of the present experiment are presented here.

The isotopically enriched ( $97.32 \pm 0.3\%$ ) thin  $^{158}\text{Gd}$  target was bombarded with a pulsed beam of  $^{28}\text{Si}$  with pulse separations of 2 and 4  $\mu\text{s}$  at energies above and below the Coulomb barrier, respectively. The thin  $^{158}\text{Gd}$  (thickness  $\approx 134.4 \mu\text{g}/\text{cm}^2$ ) target foils were fabricated on  $\approx 50 \mu\text{g}/\text{cm}^2$  carbon foil backing [36]. The targets were mounted in such

a way that carbon backing faced the beam during the experiment. The projectile energies were considered within the range of  $107 \leq E_{\text{lab}} \leq 140 \text{ MeV}$  covering  $\approx 14\%$  below to  $\approx 12\%$  above the Coulomb barrier ( $V_b^{\text{lab}} = 124.64 \text{ MeV}$ ). The recoil mass spectrometer HIRA was operated at  $\theta_{\text{lab}} = 0^\circ$  with respect to the beam direction with acceptance of 5 mSr ( $2.2^\circ$  polar angle).

Two solid-state silicon detectors with 1-mm-diameter circular aperture were mounted symmetrically at  $\theta_{\text{lab}} = 15.5^\circ$  in regard to the beam direction to monitor the beam and for normalization of the measured fusion data. To reequilibrate the charge state of the evaporation residues (ERs), 10 cm downstream from the target, a thin ( $\approx 10 \mu\text{g}/\text{cm}^2$ ) carbon foil was used. A multiwire proportional counter (MWPC) [37] of  $15 \times 5 \text{ cm}^2$  dimensions in the  $X$ – $Y$  direction was installed at the focal plane of HIRA to detect and to measure energy loss of the heavy recoiling ERs, which were transported from target chamber of HIRA based on their  $m/q$  ratio.

At the onset of the experiment, field scanning of the spectrometer was done to optimize the most probable charge state, mass, and energy of ERs at  $E_{\text{lab}} = 127.1 \text{ MeV}$ . The best setting was achieved by seeking maximum transmission efficiency and a clear separation between ERs and beamlike particles at each projectile energy. The two-dimensional spectra of ER energy loss ( $\Delta E$ ) in the MWPC vs ER time of flight (TOF) at  $E_{c.m.}/V_b = 1.12, 0.99, \text{ and } 0.86$  in Figs. 1(a)–1(c), respectively, shows a clear separation between ERs and scattered beamlike particles. Also a blank run (fields set for  $^{28}\text{Si} + ^{158}\text{Gd}$  ERs) with no target was recorded (at the lowest energy  $E_{c.m.}/V_b = 0.86$ ) for a few hours where hardly a few events were registered within the ER gated region, shown in Fig. 1(d). The CANDLER software [38] has been used to conduct offline data analysis operations.

## III. DATA ANALYSIS

Since the predicted fusion-fission cross section from the theoretical model code PACE4 [39] is negligible for  $^{28}\text{Si} + ^{158}\text{Gd}$  reaction within the studied energy window, the measured ER cross sections are assumed as the total fusion. The fusion cross sections were derived from the experimental counts using the following relation [Eq. (1)]:

$$\sigma_{\text{fus}} = \frac{1}{\epsilon} \left( \frac{Y_{\text{ER}}}{Y_M} \right) \left( \frac{d\sigma}{d\Omega} \right)_{\text{Ruth}} \Omega_{\text{norm}}, \quad (1)$$

where  $\sigma_{\text{fus}}$ ,  $Y_{\text{ER}}$ , and  $Y_M$  are the fusion cross section (mb), the yield of ERs detected at the focal plane of HIRA, and the geometric mean of yields in the two left-right monitor detectors, respectively.  $(\frac{d\sigma}{d\Omega})_{\text{Ruth}}$  is the differential Rutherford scattering cross section (mb/Sr) in the laboratory frame of reference,  $\Omega_{\text{norm}}$  (Sr) is the solid angle subtended by each monitor detector, and  $\epsilon$  is the average transmission efficiency of HIRA.

The  $\epsilon$  is defined as the ratio of the number of ERs detected at the focal plane to the number of ERs produced from the target. It is a complex function of a number of parameters, including the size of the focal plane detector, the entrance channel mass asymmetry, the projectile’s energy, the target

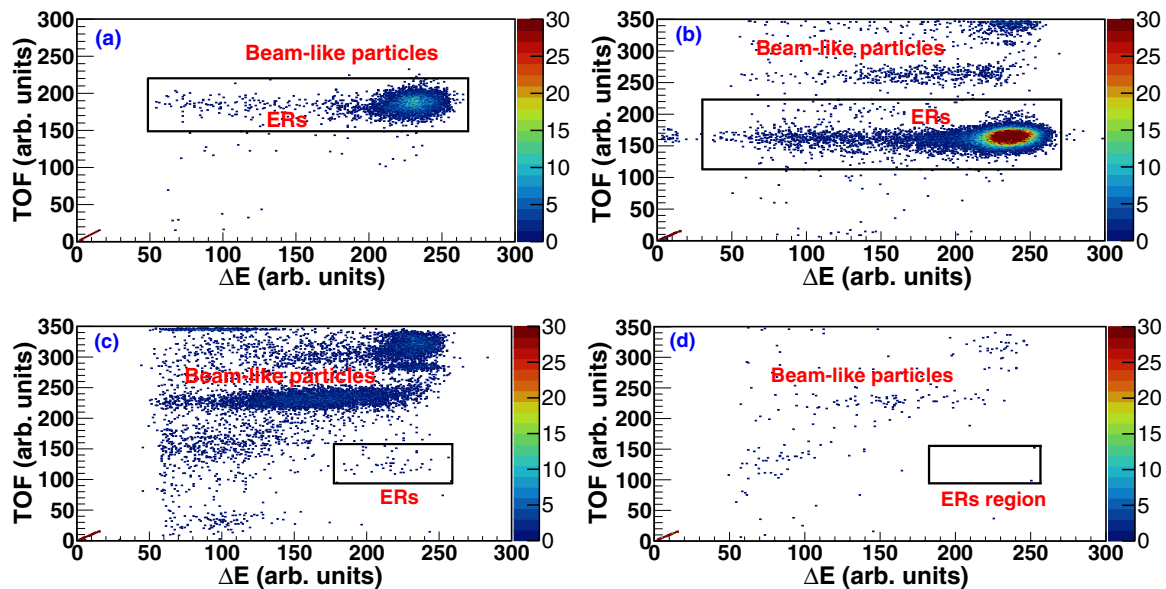


FIG. 1. Two-dimensional scatter spectra of ER energy loss ( $\Delta E$ ) in the MWPC vs ER time of flight (TOF) for  $^{28}\text{Si} + ^{158}\text{Gd}$  fusion reaction at [(a)  $E_{c.m.}/V_b = 1.12$ , (b)  $E_{c.m.}/V_b = 0.99$ , and (c)  $E_{c.m.}/V_b = 0.86$ ], and (d)  $E_{c.m.}/V_b = 0.86$  with no target. The black contours show the group of ERs that are clearly separated from scattered beamlike particles.

thickness, and the solid angle acceptance of HIRA [40]. Accordingly,  $\epsilon$  varies depending on the beam energy. The transmission efficiency of HIRA is calculated in this study using the semimicroscopic Monte Carlo code TERS [41]. The  $\approx 10\%$  uncertainty in the simulated values of HIRA efficiency is expected with respect to the measured efficiency of different systems [12,40,42]. Moreover, the possibility of the relative production of different ERs has been estimated using the statistical model code PACE4 [39] with level density parameter ( $a = A/9$ ) within the studied energy. Using the TERS code, we calculated the ER transmission efficiency of HIRA for each potential dominant ER channel at each incident energy. To estimate the average transmission efficiency ( $\epsilon$ ) of HIRA at each  $E_{lab}$ , the weighted average of HIRA efficiencies for all individual evaporation channels have been taken into account. For the current system, the calculated range of  $\epsilon$  is 5.2–8.2%. Finally, an estimated  $\epsilon$  has been used to determine the ER cross section using Eq. (1). The derived fusion cross section, except for two data points ( $E_{c.m.} = 96.0$  and  $99.5$  MeV), experienced  $< 2\%$  relative change when the level density parameter ( $a = A/10$ ) in the statistical model code PACE4 was altered. A thorough explanation of the HIRA's transmission efficiency using the TERS code can be found in Ref. [43]. The measured fusion cross sections are shown in Fig. 2 and listed in Table I with uncertainties. The corresponding uncertainty in the fusion cross section is due to (a) statistical error in ER and monitor yields, and (b) error in determining HIRA's transmission efficiency.

#### IV. RESULTS AND DISCUSSION

A comparison between the measured fusion cross section and corresponding barrier distribution (inset) of  $^{28}\text{Si} + ^{158}\text{Gd}$  and  $^{30}\text{Si} + ^{156}\text{Gd}$  [7] reactions is made on the reduced scales to eliminate the differences due to geometrical

size and barrier height, as shown in Fig. 2. Fusion BD and associated uncertainty are calculated using the three-point difference formula as prescribed in Ref. [5]. The fusion cross section and BD for  $^{30}\text{Si} + ^{156}\text{Gd}$  reaction are taken from our previous measurement [7]. The observed interesting features of Fig. 2 are (1) both systems show almost identical fusion cross sections above the Coulomb barrier energies; (2) however, enhanced fusion cross section is observed for  $^{28}\text{Si} + ^{158}\text{Gd}$  system compared to  $^{30}\text{Si} + ^{156}\text{Gd}$  [7] reaction at sub-barrier energies. This relative enhancement in  $^{28}\text{Si} + ^{158}\text{Gd}$  reaction might be due to the collective effect of static deformation of colliding partners and positive  $Q$ -value

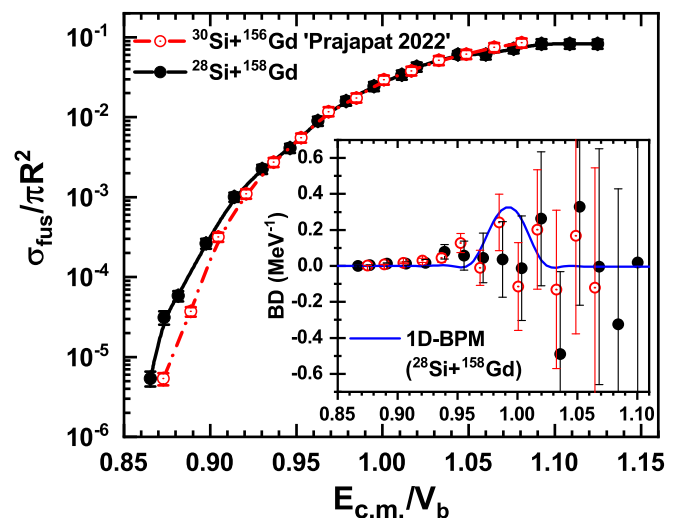


FIG. 2. The fusion excitation functions of  $^{28}\text{Si} + ^{158}\text{Gd}$  (present work) and  $^{30}\text{Si} + ^{156}\text{Gd}$ ; ‘‘Prajapat 2022’’ [7] reactions are shown on a reduced scale. The joining lines are to guide the eye. The inset represents the fusion barrier distributions of the two systems.

TABLE I. Measured fusion cross section ( $\sigma_{\text{fus}}$ ) from  $^{28}\text{Si} + ^{158}\text{Gd}$  reaction at various energies ( $E_{\text{c.m.}}$ ) and the associated uncertainties  $\delta\sigma_{\text{fus}}$ .

Energy ( $E_{\text{c.m.}}$ ) (MeV)	$\sigma_{\text{fus}} \pm \delta\sigma_{\text{fus}}$ (mb)	$E_{\text{c.m.}}$ (MeV)	$\sigma_{\text{fus}} \pm \delta\sigma_{\text{fus}}$ (mb)
90.9	$0.017 \pm 0.004$	104.6	$78.9 \pm 10.3$
91.8	$0.101 \pm 0.019$	106.3	$109.7 \pm 14.3$
92.6	$0.188 \pm 0.029$	108.0	$137.9 \pm 18.0$
94.3	$0.85 \pm 0.12$	109.7	$196.0 \pm 22.0$
96.0	$3.3 \pm 0.4$	111.4	$195.7 \pm 25.6$
97.7	$7.3 \pm 1.0$	113.1	$232.8 \pm 30.4$
99.5	$13.3 \pm 1.7$	114.8	$268.3 \pm 35.4$
101.2	$29.1 \pm 3.8$	116.5	$266.8 \pm 34.9$
102.9	$51.6 \pm 6.7$	118.2	$267.3 \pm 35.1$

neutron transfer channels. Interestingly, it can be seen from Table II that all the neutron pickup transfer (up to  $6n$ )  $Q$  values are positive in the case of  $^{28}\text{Si} + ^{158}\text{Gd}$ . In contrast, all neutron pickup channels have negative  $Q$  values except for the  $2n$  pickup case in  $^{30}\text{Si} + ^{156}\text{Gd}$  reaction. However, it is to be noted that no significant influence of the  $+2n$  transfer channel was witnessed in the  $^{30}\text{Si} + ^{156}\text{Gd}$  reaction [7]. It is also more likely for  $^{28}\text{Si}$  to pick up to  $6n$  from target to fill its outermost shell configuration  $[(1d_{5/2})^6(2S_{1/2})(1d_{3/2})]$ . A similar observation had been reported in  $^{32}\text{S} + ^{112,120}\text{Sn}$  systems [10], where  $^{32}\text{S} + ^{112}\text{Sn}$  possess all negative  $Q$  value (except for  $2n$  case) for neutron transfer channels while all were positive for  $^{32}\text{S} + ^{120}\text{Sn}$  reaction.

The BDs for both the systems  $^{28}\text{Si} + ^{158}\text{Gd}$  and  $^{30}\text{Si} + ^{156}\text{Gd}$  [7] exhibit almost similar patterns within systematic uncertainties. It is difficult to comment on the shape of BDs as the associated uncertainties are large. Moreover, CC calculations are required to deepen the understanding by considering inelastic excitations and multineutron transfer channels, which are discussed in the following sections.

### A. Coupled-channels calculations using CCFULL

To explain the fusion cross section of the  $^{28}\text{Si} + ^{158}\text{Gd}$  system, CC calculations have been performed using the CCFULL program [45]. In CCFULL, all orders of inelastic couplings are incorporated by considering vibrational couplings within the limit of harmonic oscillators and rotational ones as pure rotors. The Akyüz-Winther (AW) parametrization is taken into account to obtain the standard Woods-Saxon ion-ion potential parameters, well depth ( $V_0$ ) = 73.3 MeV, radius parameter ( $r_0$ ) = 1.18 fm, and diffuseness ( $a$ ) = 0.67 fm.

TABLE II.  $Q_{+xn}$  (MeV) values for multineutron pickup (by a projectile from target) transfer channels from the ground state (g.s.) of one to g.s. of another interacting nucleus for  $^{28,30}\text{Si} + ^{158,156}\text{Gd}$  systems.

Reaction	$Q_{+1n}$	$Q_{+2n}$	$Q_{+3n}$	$Q_{+4n}$	$Q_{+5n}$	$Q_{+6n}$
$^{30}\text{Si} + ^{156}\text{Gd}$	-1.9	+0.8	-3.6	-2.3	-8.4	-8.8
$^{28}\text{Si} + ^{158}\text{Gd}$	+0.5	+4.7	+2.8	+5.6	+1.2	+2.4

TABLE III. Excited states ( $\lambda^\pi$ ) with excitation energies ( $E^*$ ) and corresponding deformation parameters ( $\beta_\lambda$ ) [12,44] of  $^{28}\text{Si}$  and  $^{158}\text{Gd}$  used in the coupled-channels calculations.

Nucleus	$E^*$ (MeV)	$\lambda^\pi$	$\beta_\lambda$
$^{28}\text{Si}$	1.779	$2^+$	-0.407
	4.618	$4^+$	0.187
$^{158}\text{Gd}$	0.795	$2^+$	0.282
	0.2615	$4^+$	0.082

However, these parameters are adjusted to  $V_0 = 80.0$  MeV,  $r_0 = 1.15$  fm, and  $a = 0.776$  fm to fit the above barrier data and to obtain the corresponding equivalent uncoupled barrier parameters, barrier height ( $V_b$ ) = 105.09 MeV, barrier radius ( $r_b$ ) = 11.34 fm, and curvature = 3.81 MeV. The low-lying collective states, excitation energy, and corresponding deformation of projectile and target are reported in Table III.

Figure 3 shows the comparison of measured fusion data [Fig. 3(a)] and extracted fusion barrier distribution [Fig. 3(b)] with theoretical calculations by considering no coupling (1D-BPM) and coupling of various rotational states of the projectile (P)  $^{28}\text{Si}$  and target (T)  $^{158}\text{Gd}$  nuclei. The measured sub-barrier fusion cross section is much larger than the 1D-BPM (no coupling limit). To improve the prediction, we assumed  $^{28}\text{Si}$  as inert and included coupling of various states in the rotational band (NRot = 1, 2, 3, and 4) of  $^{158}\text{Gd}$  one after other but reported only NRot = 4 in Fig. 3 to avert the crowd. NRot is defined as the number of levels in the rotational band to be included (up to  $2^*\text{NRot}^+$  states) along with ground state, e.g., if NRot = 4, then  $0^+$ ,  $2^+$ ,  $4^+$ ,  $6^+$ , and

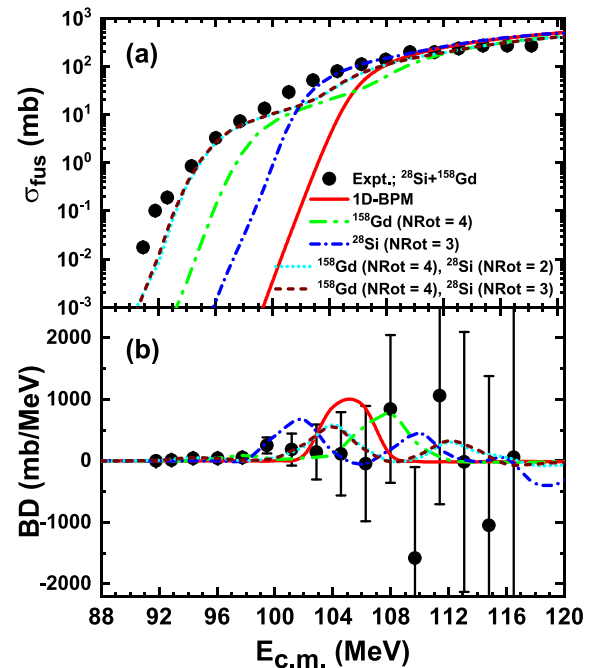


FIG. 3. The comparison between the measured fusion data (top panel), extracted barrier distribution (bottom panel), and results obtained from coupled-channels code CCFULL for  $^{28}\text{Si} + ^{158}\text{Gd}$  reaction (see text for the details).

$8^+$  states are considered. The result from such calculations enhanced the sub-barrier fusion cross sections. In the next step, the coupling of different rotational states of  $^{28}\text{Si}$  was tested by considering  $\text{NRot} = 1$  to 3, though depicted only  $\text{NRot} = 3$  in Fig. 3. The  $0^+$ ,  $2^+$ ,  $4^+$ , and  $6^+$  states of  $^{28}\text{Si}$  enhanced the sub-barrier fusion cross section marginally as compared to couplings in the target. It is essential to note that further inclusion of rotational states in target ( $\text{NRot} = 5$ ) and projectile ( $\text{NRot} = 4$ ) did not alter the sub-barrier cross section. It suggests that individual couplings in colliding nuclei are insufficient to reproduce the fusion and BD data at below-barrier energies. As a result, the combined effect of P and T was considered. Hence, the CC calculations with rotational states from  $\text{NRot} = 4$  in  $^{158}\text{Gd}$  and  $\text{NRot} = 2$  and 3 in  $^{28}\text{Si}$  are shown in Fig. 3. The theoretical predictions for fusion cross section and BD are almost similar in both cases, indicating the significant role of rotational states up to  $0^+$ ,  $2^+$ , and  $4^+$  in  $^{28}\text{Si}$ . Including combined couplings in P-T nuclei brings in an additional enhancement and provides a good fit to the data except for the three lowest energy points and in  $E_{\text{c.m.}} = 99\text{--}106$  MeV region. The combination of CC calculations is consistent with the extracted BD within the experimental uncertainties over the energy range.

The energy of  $4^+$  state (4.618 MeV) of  $^{28}\text{Si}$  lies in the middle of the vibrational prediction ( $2 \times 1.78 = 3.56$  MeV) and rotational estimate ( $3.33 \times 1.78 = 5.93$  MeV), where 1.78 MeV is the experimental energy of  $2^+$  state. Hence, it is unclear which couplings (rotational/vibrational) in  $^{28}\text{Si}$  are more appropriate to explain the fusion data and subsequent BD. Therefore, CC calculations were also performed considering vibrational couplings in the projectile and rotational excitations in the target, displayed in Figs. 4(a) and 4(b). A comparison is made by considering the  $2^+$  state with one and two phonons (1ph and 2ph) in  $^{28}\text{Si}$  and rotational excitations in target ( $\text{NRot} = 4$ ; optimum value). One can notice that consideration of 2ph  $2^+$  state of  $^{28}\text{Si}$  enhances the magnitude of sub-barrier fusion cross section in comparison to 1ph  $2^+$  state in projectile along with rotational couplings in the target. However, the result of such predictions could not reproduce the measured cross section at the three lowest energy points and around the Coulomb barrier ( $E_{\text{c.m.}} = 96\text{--}110$  MeV). It was pointed out in Ref. [46] that the  $3^-$  state of  $^{28}\text{Si}$  is high in energy (6.878 MeV); thus, it was not expected to play any significant role in CC calculations. However, to make the comparison with  $^{30}\text{Si} + ^{156}\text{Gd}$  reaction on equal footing, where we had considered the  $^{156}\text{Gd}$  ( $\text{NRot} = 4$ ) +  $^{30}\text{Si}$  ( $2^+$ ,  $3^-$ ) couplings (see Fig. 5(b) in Ref. [7]) in the colliding partners, we have included  $3^-$  state of  $^{28}\text{Si}$  in the current study. We found that the inclusion of one phonon in  $2^+$  and  $3^-$  states of  $^{28}\text{Si}$ , along with rotational excitations in target, could not improve the fitting of fusion excitation function in the sub-barrier zone.

Based on the above analysis, it could be pointed out that treating  $^{28}\text{Si}$  as a rotor rather than a vibrator gives a somewhat better fit to the measured excitation function, and BD is consistent within experimental uncertainties. In literature, fusion data appears to be explained in most cases by considering coupling to rotational excitations in  $^{28}\text{Si}$  [12,47].

It is to be noted that even after incorporating the full-fledged collective excitations in colliding nuclei, all

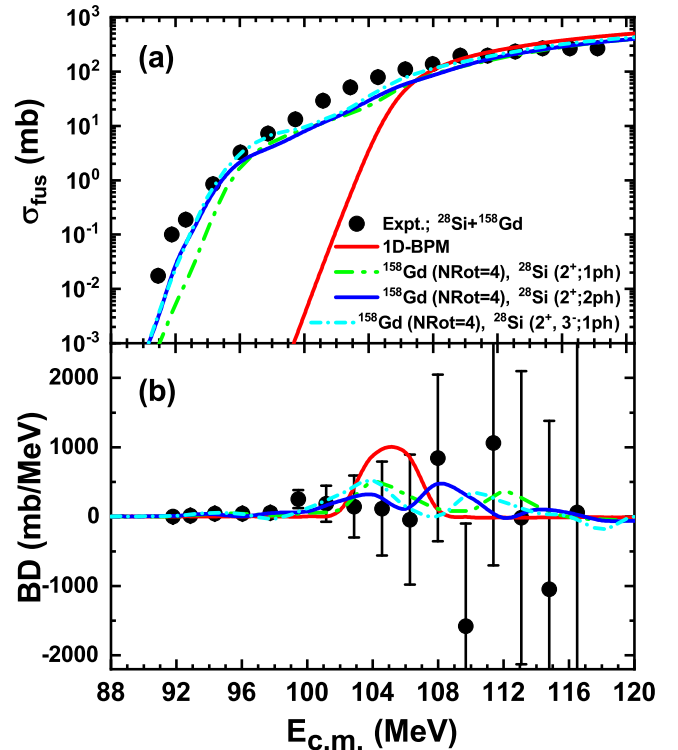


FIG. 4. Same as Fig. 3 with vibrational couplings in  $^{28}\text{Si}$  and rotational excitations in  $^{158}\text{Gd}$  (see text for the details).

failed to explain the fusion data in deep sub-barrier energy region, indicating the necessity of multineutron transfer couplings with positive  $Q$  value (see Table II).

### B. Empirical channel coupling calculations using ECC

Since CCFUL with various inelastic excitations in colliding nuclei could not explain the fusion excitation function throughout the energy range, the ECC approach was adopted. ECC model was proposed by Zagrebaev *et al.* [22], which allows incorporating multineutron rearrangement/transfer channel couplings along with inelastic excitations in colliding partners. Within this model, the incoming flux may penetrate the multidimensional Coulomb barrier in the channels with different intermediate neutron transfers. More details about ECC formalism can be found in Refs. [48,49].

ECC calculations have been performed using the Woods-Saxon ion-ion potential with AW parameters  $V_0 = 80.0$  MeV,  $r_0 = 1.16$  fm, and  $a = 0.78$  fm. The coupling strength parameters for rotational excitations in projectile and target nuclei used in the calculation are tabulated in Table III.

A comparison has been made between the experimental fusion cross section [Fig. 5(a)] and those predicted from the ECC model for  $^{28}\text{Si} + ^{158}\text{Gd}$  reaction and similarly for BD in Fig. 5(b). We first considered 1D-BPM (uncoupled) and ECC without neutron transfer in its calculation kernel. Later, neutron transfer channels with positive  $Q$  values and collective excitations in P-T nuclei were taken into account one by one (see Fig. 5). It can be observed that ECC calculations with up to  $2n$  transfer are in good agreement with the measured fusion

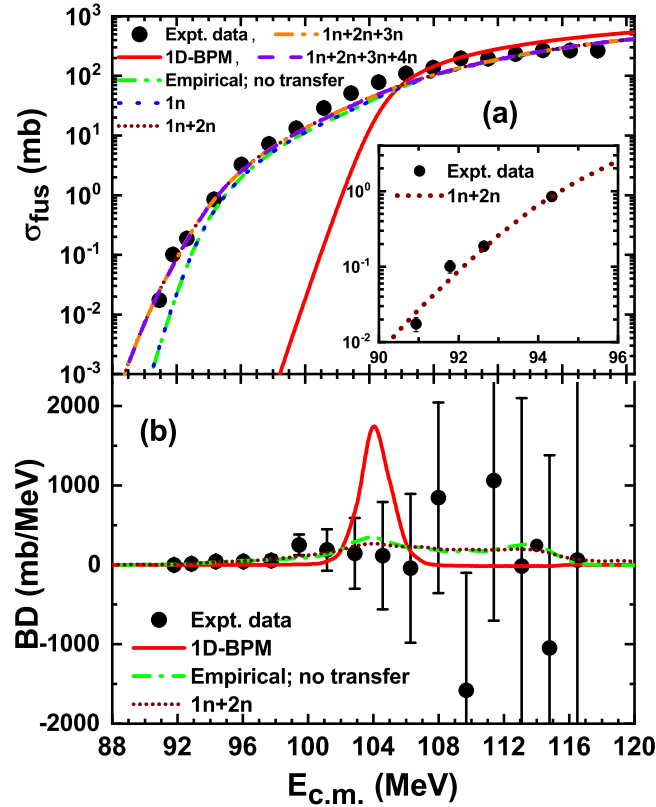


FIG. 5. Same as Fig. 3 with theoretical calculations from the ECC program (see text for the details).

data throughout the energy range, except at  $E_{c.m.} = 90.9, 91.8$ , and around  $E_{c.m.} = 103$  MeV. The slight deviation between the experimental cross section and theoretical estimation [see inset of Fig. 5(a)] may be an indication of fusion hindrance at extreme sub-barrier energy ( $E_{c.m.} = 90.9$  MeV). The investigation of fusion hindrance is presented in the next section. Interestingly, the experimental fusion BD is consistent with ECC calculations. This may indicate the role of  $2n$  transfer with  $Q > 0$  on sub-barrier fusion. However, further inclusion of  $3n$  and  $4n$  transfer channels did not alter the fusion cross section, which describes the insignificant role of multinucleon transfer (more than  $2n$ ) on fusion data in the present study. The situation is quite similar to previous studies [48,50] where transfer channels with positive  $Q$  values were found significant up to  $2n$ . However, the slight wideness in the fusion BD due to transfer channels along with inelastic excitations is reported in Ref. [49].

### C. Investigation of fusion hindrance

At extreme sub-barrier energies, astrophysical  $S(E_{c.m.})$  factor and logarithmic derivative  $L(E_{c.m.})$  factor are convenient components for characterizing the discrepancy between experimental and theoretical fusion EFs. The factors are defined as [1,24,30]

$$S(E_{c.m.}) = E_{c.m.} \sigma_{\text{fus}}(E_{c.m.}) \exp[2\pi(\eta - \eta_0)], \quad (2)$$

$$L(E_{c.m.}) = \frac{d[\ln(E_{c.m.} \sigma_{\text{fus}})]}{dE_{c.m.}} = \frac{1}{E_{c.m.} \sigma_{\text{fus}}} \frac{d(E_{c.m.} \sigma_{\text{fus}})}{dE_{c.m.}}, \quad (3)$$

where  $\eta = Z_1 Z_2 e^2 \sqrt{\mu / (2E_{c.m.} \hbar^2)}$  is the Sommerfeld parameter ( $\mu$  is reduced mass of the system,  $Z_1$  and  $Z_2$  are projectile and target charge numbers, respectively). We introduce a constant  $\eta_0$  ( $\eta = \eta_0$  at  $E_{c.m.} = V_b$ ) in the exponent to make the presentation more apparent.

The experimental and theoretical representation of  $S(E_{c.m.})$  factor is shown in Fig. 6(a). The CC [ $^{158}\text{Gd}$  (NRot = 4) +  $^{28}\text{Si}$  (NRot = 3)] predictions are in good agreement with the experimental  $S(E_{c.m.})$  factor, except for a few lowest energy points, and reflect a good description of  $S(E_{c.m.})$  factor. However, it can also be noticed that the experimental  $S(E_{c.m.})$  factor is not exhibiting the maximum, but CC (ECC with  $1n + 2n$ ) calculations are above the experimental  $S(E_{c.m.})$  factor at the lowest energy point [see inset of Fig. 6(a)] while reproducing it well towards higher energy zone. This may suggest the presence of fusion hindrance in the  $^{28}\text{Si} + ^{158}\text{Gd}$  reaction at deep sub-barrier energies. However, additional experimental data at low energies are required to be more specific. Note that a similar scenario was reported in the literature [18,30,51]. Moreover, it is worth mentioning that  $^{28}\text{Si}$  is a soft nucleus (i.e., well deformed), and additional influence of one and two neutron transfers with positive  $Q$  value is observed in  $^{28}\text{Si} + ^{158}\text{Gd}$  reaction. This fact could result in different turning points based on the mutual orientation of colliding nuclei that may lead to multiple barriers. Hence, such transfer couplings and nuclear structural peculiarities of colliding partners can push down the  $S(E_{c.m.})$ -factor maximum or even vanish it as also observed in  $^{48}\text{Ti} + ^{58}\text{Fe}$  reaction [30]. Moreover, additional experimental data are required at deep sub-barrier energies to delineate the  $S(E_{c.m.})$ -factor maximum for the  $^{28}\text{Si} + ^{158}\text{Gd}$  system.

Another indirect method to illustrate the fusion hindrance is the logarithmic derivative  $L(E_{c.m.})$  of the energy-weighted cross section, which is defined by Eq. (3) and estimated using the two-point difference method. As it has been argued [24], the  $S$ -factor maximum appears when  $L(E_{c.m.})$  reaches the constant  $S(E_{c.m.})$ -factor value,  $L_{CS}(E_{c.m.}) = \pi \eta / E_{c.m.}$ , and the energy ( $E_S$ ) at which  $L_{CS}(E_{c.m.})$  intersect the  $L(E_{c.m.})$  is termed as the experimental threshold energy for fusion hindrance. A comparison between experimental and theoretical results of the  $L(E_{c.m.})$  factor is shown in Fig. 6(b). As seen, the experimental and theoretical [ $^{158}\text{Gd}$  (NRot = 4) +  $^{28}\text{Si}$  (NRot = 3)] logarithmic slopes have a steeply rising trend with the decreasing energy around and below the barrier. In the deep sub-barrier region,  $L(E_{c.m.})$  has a very narrow maximum; a similar behavior was revealed in a more symmetric system,  $^{48}\text{Ti} + ^{58}\text{Fe}$  [30]. Contrary to that, no such maximum is observed in theoretical ECC predictions with one and two neutron transfer channels, and the logarithmic slope has increasing behavior with decreasing energy throughout the energy window. It may be the effect of strong transfer couplings in the deep sub-barrier region. Also, it has already been exhibited that there is a crossover between  $L_{CS}(E_{c.m.})$  line and the experimental  $L(E_{c.m.})$  in those systems, which revealed the signature of fusion hindrance [1,3,25]. In the present study, the  $L_{CS}(E_{c.m.})$  line is intersecting the experimental  $L(E_{c.m.})$  at energy  $E_{c.m.} = 92.6$  MeV, which is the experimental threshold energy ( $E_S$ ) of fusion hindrance.

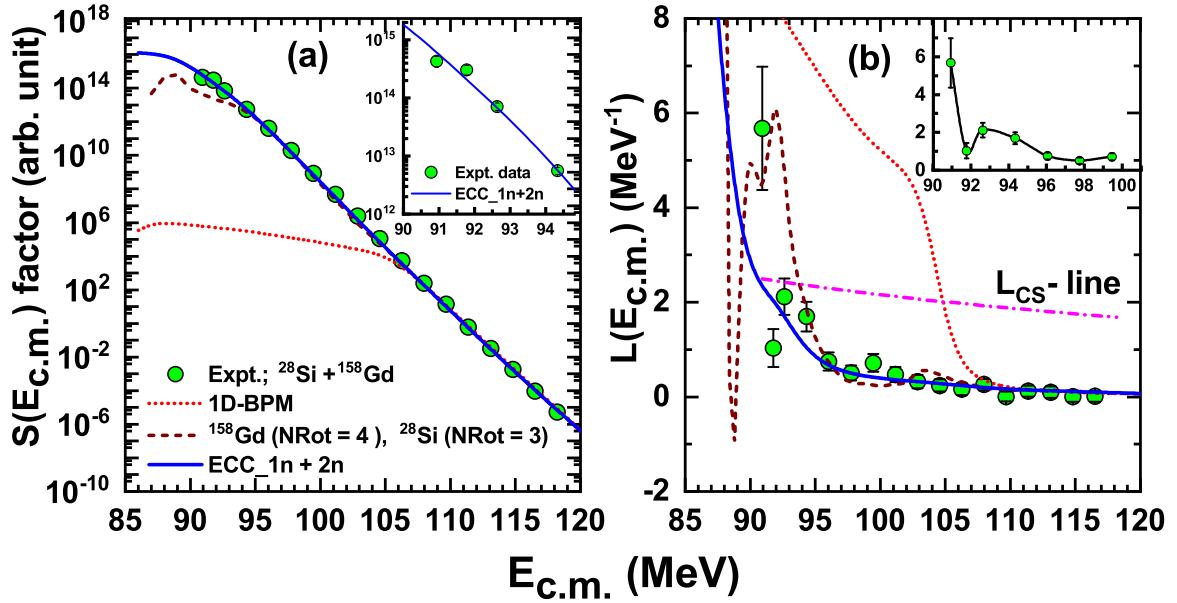


FIG. 6. Experimentally derived and theoretically predicted (a) astrophysical  $S(E_{c.m.})$  factor and (b)  $L(E_{c.m.})$  factor for  $^{28}\text{Si} + ^{158}\text{Gd}$  system. The insets show the closer visualization of excitation functions in the deep sub-barrier region.

Further, we have calculated the logarithmic slope  $L(E_{c.m.})$  for the  $^{30}\text{Si} + ^{156}\text{Gd}$  system using the measured fusion data from Ref. [7] and compared with the  $^{28}\text{Si} + ^{158}\text{Gd}$  reaction (present study) on a normalized energy scale in Fig. 7. Both systems depict similar behavior except at the lowest energy points, possibly due to the structural effect of two different projectiles ( $^{28,30}\text{Si}$ ) and neutron transfer channels. In the case of the  $^{30}\text{Si} + ^{156}\text{Gd}$  reaction,  $L(E_{c.m.})$  is grossly rising with decreasing energy and fusion excitation functions (see Ref. [7]) are well reproduced by CC predictions, which indicates no signature of fusion hindrance within the studied

energy window. A similar discussion has been made for  $^{64,60}\text{Ni} + ^{100}\text{Mo}$  [18,25], containing a set of positive and negative neutron transfer  $Q$  values, the onset of fusion hindrance is witnessed in  $^{64}\text{Ni} + ^{100}\text{Mo}$  system which has a positive  $Q$  value for  $2n$  transfer only, which is opposite to the current study for  $^{28,30}\text{Si} + ^{158,156}\text{Gd}$  reactions.

Furthermore, threshold energy ( $E_S$ ) for fusion hindrance is estimated using the following empirical formula [Eq. (4)]:

$$E_S(\zeta) = 0.356\zeta^{2/3} \text{ MeV}, \quad (4)$$

where  $\zeta = Z_p Z_t \sqrt{A_p A_t / (A_p + A_t)}$  is the entrance channel parameter which is characterizing the size of the colliding partners.  $Z_p - Z_t$  and  $A_p - A_t$  are the charge and mass numbers of projectile-target nuclei. However, it is to be noted that this systematic relation for  $E_S$  [Eq. (4)] was derived for the stiff colliding partners and provides an upper limit for the soft systems. A systematic comparison is made between the experimentally obtained  $E_S$  [crossing point between  $L_{CS}(E_{c.m.})$  line and  $L(E_{c.m.})$ ] and the empirically estimated values [Eq. (4)] for symmetric ( $^{64}\text{Ni} + ^{100}\text{Mo}$  [25],  $^{60}\text{Ni} + ^{89}\text{Y}$  [23],  $^{64}\text{Ni} + ^{64}\text{Ni}$  [24],  $^{28}\text{Si} + ^{30}\text{Si}$  [52], and  $^{28}\text{Si} + ^{64}\text{Ni}$  [28]) and asymmetric reactions ( $^{11}\text{B} + ^{197}\text{Au}$  [26],  $^{12}\text{C} + ^{198}\text{Pt}$  [29], and  $^{16}\text{O} + ^{208}\text{Pb}$  [27]) in which the reaction partners are soft and/or stiff nuclei. It can be seen from Fig. 8 that all the systems follow the systematics, including present measurement. The deviation from the empirical line can be observed for  $^{64}\text{Ni} + ^{100}\text{Mo}$  and  $^{64}\text{Ni} + ^{64}\text{Ni}$  systems which have open-shell soft nuclei leading to the strong coupling effect in broadening the BD and pushing down the threshold for fusion hindrance. This reflects a good correlation between the entrance channel parameter ( $\zeta$ ) and threshold for fusion hindrance, which is nicely fitted by the empirical formula for different systems (see Fig. 8) including  $^{28}\text{Si} + ^{158}\text{Gd}$  (present study).

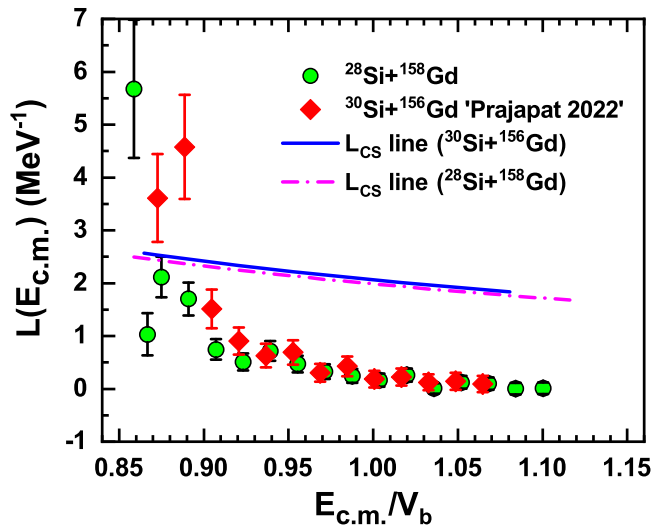


FIG. 7. The logarithmic derivatives (slopes) of the excitation functions for the two systems;  $^{28}\text{Si} + ^{158}\text{Gd}$  (present study) and for  $^{30}\text{Si} + ^{156}\text{Gd}$  reaction ‘‘Prajapat 2022’’ [7] on the reduced energy scale.

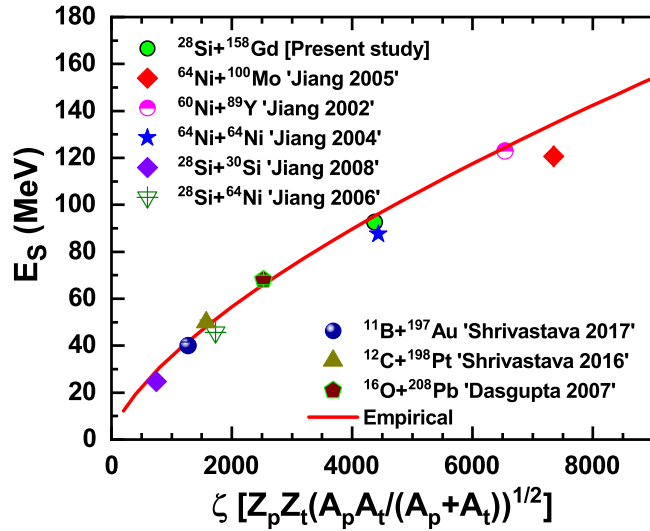


FIG. 8. Comparison between the experimental and empirically [Eq. (4)] obtained fusion hindrance threshold energy ( $E_S$ ) as a function of entrance channel parameter ( $\zeta$ ) for  $^{28}\text{Si} + ^{158}\text{Gd}$  (present study),  $^{64}\text{Ni} + ^{100}\text{Mo}$  “Jiang 2005” [25],  $^{60}\text{Ni} + ^{89}\text{Y}$  “Jiang 2002” [23],  $^{64}\text{Ni} + ^{64}\text{Ni}$  “Jiang 2004” [24],  $^{28}\text{Si} + ^{30}\text{Si}$  “Jiang 2008” [52],  $^{28}\text{Si} + ^{64}\text{Ni}$  “Jiang 2006” [28],  $^{11}\text{B} + ^{197}\text{Au}$  “Shrivastava 2017” [26],  $^{12}\text{C} + ^{198}\text{Pt}$  “Shrivastava 2016” [29], and  $^{16}\text{O} + ^{208}\text{Pb}$  “Dasgupta 2007” [27] systems.

## V. CONCLUSION

In this article, we reported the fusion excitation function for  $^{28}\text{Si} + ^{158}\text{Gd}$  reaction at energies around and deep below the Coulomb barrier ( $\approx 14\%$  down). The experimental data have been analyzed within the coupled-channels formalism by considering  $^{28}\text{Si}$  as a rotor (also vibrator) and  $^{158}\text{Gd}$  as a rotor within the framework of CCFULL and ECC programs. The rotational couplings in projectile and target nuclei significantly enhance the fusion cross section at energies around the Coulomb barrier but failed to reproduce the data in the extreme sub-barrier region. Since the system has positive  $Q$  values for the neutron pickup channels (up to  $6n$ ), the transfer coupling along with collective excitations are examined using the ECC model. Including up to  $2n$  transfer channel grossly reproduces the measured fusion excitation function (except at  $E_{c.m.} = 90.9, 91.8$ , and around  $E_{c.m.} = 103$  MeV) and corresponding BD. The deviation between the standard CC calculations and experimental data

at deep sub-barrier energy point may indicate the threshold for the fusion hindrance in  $^{28}\text{Si} + ^{158}\text{Gd}$  reaction, but additional experimental data at low energies are required for conclusive remark. Besides, the influence of multineutron pickup transfer channels (more than two neutrons) having positive  $Q$  values is not established for  $^{28}\text{Si} + ^{158}\text{Gd}$  system.

Furthermore, to interpret the fusion excitation function at extreme sub-barrier energies,  $S(E_{c.m.})$  and  $L(E_{c.m.})$  factors have been extracted for  $^{28}\text{Si} + ^{158}\text{Gd}$  reaction. No maximum in  $S(E_{c.m.})$  factor is observed, which might be washed out due to well-deformed colliding nuclei and transfer channel couplings. However, a well-pronounced maximum in  $L(E_{c.m.})$  factor is exhibited, and the logarithmic slope increases with decreasing the energy except for a few deep sub-barrier energy points. Experimentally obtained threshold energy for fusion hindrance agrees with the empirical formula. We have also compared the experimental fusion hindrance threshold as a function of the entrance channel parameter with the empirical formula for different symmetric and asymmetric systems, including our measurements. Except for a few systems, there is a good consistency between the experimental and empirical values.

A qualitative comparison between  $^{28}\text{Si} + ^{158}\text{Gd}$  reaction and  $^{30}\text{Si} + ^{156}\text{Gd}$  [7], leading to the same compound nucleus  $^{186}\text{Pt}^*$ , provides the following conclusions: (i) the measured sub-barrier fusion cross section is larger for the  $^{28}\text{Si} + ^{158}\text{Gd}$  than  $^{30}\text{Si} + ^{156}\text{Gd}$ , indicating the role of neutron transfer (up to  $2n$ ) with positive  $Q$  values in the first system, (ii) no evidence of fusion hindrance has been observed in  $^{30}\text{Si} + ^{156}\text{Gd}$  reaction as the  $L(E_{c.m.})$  is grossly increasing with decreasing energy. More experimental data are needed in the deep sub-barrier zone to conclude on fusion hindrance in  $^{30}\text{Si} + ^{156}\text{Gd}$  reaction.

## ACKNOWLEDGMENTS

We thank the IUAC Pelletron team for their cooperation during the experiment and the IUAC target laboratory group for helping in target preparation. We also thank E. M. Kozulin and D. Kumar from FLNR, Dubna, Russia, for their cooperation and support towards the Indo-Russian project, which allowed us to obtain the enriched target material. M.M. acknowledges Research Grant No. INT/RUS/RFBR/387 from DST(IN). Student research fellowships from MHRD and DST-INSPIRE (IF180078), Department of Science and Technology, Ministry of Science and Technology Government of India, are also gratefully acknowledged.

[1] C. L. Jiang, B. B. Back, K. E. Rehm, K. Hagino, G. Montagnoli, and A. M. Stefanini, *Eur. Phys. J. A* **57**, 235 (2021).  
 [2] Tea Mijatović, *Front. Phys.* **10**, 965198 (2022).  
 [3] B. B. Back, H. Esbensen, C. L. Jiang, and K. E. Rehm, *Rev. Mod. Phys.* **86**, 317 (2014).  
 [4] M. Beckerman, *Rep. Prog. Phys.* **51**, 1047 (1988).  
 [5] M. Dasgupta, D. J. Hinde, N. Rowley, and A. M. Stefanini, *Annu. Rev. Nucl. Part. Sci.* **48**, 401 (1998).

[6] A. Chauhan, R. Prajapat, G. Sarkar, M. Maiti, R. Kumar, Malvika, Gonika, J. Gehlot, S. Nath, A. Parihari, and N. Madhavan, *Phys. Rev. C* **102**, 064606 (2020).  
 [7] R. Prajapat, M. Maiti, R. Kumar, M. Sagwal, Gonika, C. Kumar, R. Biswas, J. Gehlot, S. Nath, and N. Madhavan, *Phys. Rev. C* **105**, 064612 (2022).  
 [8] D. Kumar, M. Maiti, R. Prajapat, A. Chauhan, R. Biswas, J. Gehlot, S. Nath, R. Kumar, N. Madhavan, G. N. Jyothi *et al.*, *Phys. Rev. C* **104**, 014602 (2021).



- [9] A. M. Stefanini, G. Montagnoli, M. D'Andrea, M. Giacomini, C. Dehman, R. Somasundaram, V. Vijayan, L. Zago, G. Colucci, F. Galtarossa *et al.*, *J. Phys. G: Nucl. Part. Phys.* **48**, 055101 (2021).
- [10] V. Tripathi, L. T. Baby, J. J. Das, P. Sugathan, N. Madhavan, A. K. Sinha, P. V. Madhusudhana Rao, S. K. Hui, R. Singh, and K. Hagino, *Phys. Rev. C* **65**, 014614 (2001).
- [11] M. Beckerman, M. Salomaa, A. Sperduto, H. Enge, J. Ball, A. Di Rienzo, S. Gazes, Y. Chen, J. D. Molitoris, and Mao Naifeng, *Phys. Rev. Lett.* **45**, 1472 (1980).
- [12] S. Kalkal, S. Mandal, N. Madhavan, E. Prasad, S. Verma, A. Jhingan, R. Sandal, S. Nath, J. Gehlot, B. R. Behera *et al.*, *Phys. Rev. C* **81**, 044610 (2010).
- [13] C. L. Jiang, K. E. Rehm, B. B. Back, H. Esbensen, R. V. F. Janssens, A. M. Stefanini, and G. Montagnoli, *Phys. Rev. C* **89**, 051603(R) (2014).
- [14] F. Scarlassara, S. Beghini, G. Montagnoli, G. F. Segato, D. Ackermann, L. Corradi, C. J. Lin, A. M. Stefanini, and L. F. Zheng, *Nucl. Phys. A* **672**, 99 (2000).
- [15] G. Montagnoli, A. M. Stefanini, H. Esbensen, C. L. Jiang, L. Corradi, S. Courtin, E. Fioretto, J. Grebosz, F. Haas, H. M. Jia *et al.*, *Phys. Rev. C* **90**, 044608 (2014).
- [16] N. K. Deb, K. Kalita, H. A. Rashid, S. Nath, J. Gehlot, N. Madhavan, R. Biswas, R. N. Sahoo, P. K. Giri, A. Das *et al.*, *Phys. Rev. C* **102**, 034603 (2020).
- [17] H. M. Jia, C. J. Lin, F. Yang, X. X. Xu, H. Q. Zhang, Z. H. Liu, L. Yang, S. T. Zhang, P. F. Bao, and L. J. Sun, *Phys. Rev. C* **86**, 044621 (2012).
- [18] A. M. Stefanini, G. Montagnoli, F. Scarlassara, C. L. Jiang, H. Esbensen, E. Fioretto, L. Corradi, B. B. Back, C. M. Deibel, and B. Di Giovine, *Eur. Phys. J. A* **49**, 63 (2013).
- [19] Z. Kohley, J. F. Liang, D. Shapira, R. L. Varner, C. J. Gross, J. M. Allmond, A. L. Caraley, E. A. Coello, F. Favela, K. Lagergren *et al.*, *Phys. Rev. Lett.* **107**, 202701 (2011).
- [20] P. H. Stelson, *Phys. Lett. B* **205**, 190 (1988).
- [21] P. H. Stelson, H. J. Kim, M. Beckerman, D. Shapira, and R. L. Robinson, *Phys. Rev. C* **41**, 1584 (1990).
- [22] V. I. Zagrebaev, *Phys. Rev. C* **64**, 034606 (2001); **67**, 061601(R) (2003).
- [23] C. L. Jiang, H. Esbensen, K. E. Rehm, B. B. Back, R. V. F. Janssens, J. A. Caggiano, P. Collon, J. Greene, A. M. Heinz, D. J. Henderson *et al.*, *Phys. Rev. Lett.* **89**, 052701 (2002).
- [24] C. L. Jiang, K. E. Rehm, R. V. F. Janssens, H. Esbensen, I. Ahmad, B. B. Back, P. Collon, C. N. Davids, J. P. Greene, D. J. Henderson *et al.*, *Phys. Rev. Lett.* **93**, 012701 (2004).
- [25] C. L. Jiang, K. E. Rehm, H. Esbensen, R. V. F. Janssens, B. B. Back, C. N. Davids, J. P. Greene, D. J. Henderson, C. J. Lister *et al.*, *Phys. Rev. C* **71**, 044613 (2005).
- [26] A. Shrivastava, K. Mahata, V. Nanal, S. K. Pandit, V. V. Parkar, P. C. Rout, N. Dokania, K. Ramachandran, A. Kumar, A. Chatterjee *et al.*, *Phys. Rev. C* **96**, 034620 (2017).
- [27] M. Dasgupta, D. J. Hinde, A. Diaz-Torres, B. Bouriquet, Catherine I. Low, G. J. Milburn, and J. O. Newton, *Phys. Rev. Lett.* **99**, 192701 (2007).
- [28] C. L. Jiang, B. B. Back, H. Esbensen, R. V. F. Janssens, Ş. Mişicu, K. E. Rehm, P. Collon, C. N. Davids, J. Greene, and D. J. Henderson, *Phys. Lett. B* **640**, 18 (2006).
- [29] A. Shrivastava, K. Mahata, S. K. Pandit, V. Nanal, T. Ichikawa, K. Hagino, A. Navin, C. S. Palshetkar, V. V. Parkar, K. Ramachandran, P. C. Rout *et al.*, *Phys. Lett. B* **755**, 332 (2016).
- [30] V. V. Sargsyan, G. G. Adamian, N. V. Antonenko, W. Scheid, and H. Q. Zhang, *Phys. Rev. C* **95**, 054619 (2017).
- [31] Md M. Shaikh, S. Nath, J. Gehlot, T. Banerjee, I. Mukul, R. Dubey, A. Shamlath, P. V. Laveen, M. Shareef, A. Jhingan *et al.*, *J. Phys. G: Nucl. Part. Phys.* **45**, 095103 (2018).
- [32] C. Simenel, A. S. Umar, K. Godbey, M. Dasgupta, and D. J. Hinde, *Phys. Rev. C* **95**, 031601(R) (2017).
- [33] T. Ichikawa, *Phys. Rev. C* **92**, 064604 (2015).
- [34] T. Ichikawa and K. Matsuyanagi, *Phys. Rev. C* **92**, 021602(R) (2015).
- [35] A. K. Sinha, N. Madhavan, J. J. Das, P. Sugathan, D. O. Kataria, A. P. Patro, and G. K. Mehta, *Nucl. Instrum. Methods A* **339**, 543 (1994).
- [36] R. Prajapat, M. Maiti, S. R. Abhilash, G. R. Umaphathy, D. Kabiraj, S. A. Khan, D. Khandelwal, and A. Dawar, *Vacuum* **201**, 111033 (2022).
- [37] J. Gehlot, A. Jhingan, T. Varughese, S. Nath, and N. Madhavan, DAE Symp. on Nucl. Phys. **65**, 782 (2021).
- [38] E. T. Subramaniam, B. P. Ajith Kumar, and R. K. Bhowmik, Collection and analysis of nuclear data using Linux network (unpublished).
- [39] A. Gavron, *Phys. Rev. C* **21**, 230 (1980).
- [40] S. Nath, P. V. Madhusudhana Rao, S. Pal, J. Gehlot, E. Prasad, G. Mohanto, S. Kalkal, J. Sadhukhan, P. D. Shidling, K. S. Golda, A. Jhingan, N. Madhavan, S. Muralithar, and A. K. Sinha, *Phys. Rev. C* **81**, 064601 (2010).
- [41] S. Nath, *Comput. Phys. Commun.* **179**, 492 (2008); **180**, 2392 (2009).
- [42] N. V. S. V. Prasad, A. M. Vinodkumar, A. K. Sinha, K. M. Varier, D. L. Sastry, N. Madhavan, P. Sugathan, D. O. Kataria, and J. J. Das, *Nucl. Phys. A* **603**, 176 (1996).
- [43] S. Nath, *Nucl. Instrum. Methods Phys. A* **576**, 403 (2007).
- [44] P. Möller, A. J. Sierk, T. Ichikawa, and H. Sagawa, *At. Data Nucl. Data Tables* **109-110**, 1 (2016).
- [45] K. Hagino, N. Rowley, and T. Kruppa, *Comput. Phys. Commun.* **123**, 143 (1999).
- [46] K. Hagino, N. Takigawa, J. R. Bennett, and D. M. Brink, *Phys. Rev. C* **51**, 3190 (1995).
- [47] J. O. Newton, C. R. Morton, M. Dasgupta, J. R. Leigh, J. C. Mein, D. J. Hinde, H. Timmers, and K. Hagino, *Phys. Rev. C* **64**, 064608 (2001).
- [48] V. A. Rachkov, A. V. Karpov, A. S. Denikin, and V. I. Zagrebaev, *Phys. Rev. C* **90**, 014614 (2014).
- [49] H. Q. Zhang, C. J. Lin, F. Yang, H. M. Jia, X. X. Xu, Z. D. Wu, F. Jia, S. T. Zhang, Z. H. Liu, A. Richard *et al.*, *Phys. Rev. C* **82**, 054609 (2010).
- [50] Khushboo, N. Madhavan, S. Nath, A. Jhingan, J. Gehlot, B. Behera, S. Verma, S. Kalkal, and S. Mandal, *Phys. Rev. C* **100**, 064612 (2019).
- [51] A. M. Stefanini, G. Montagnoli, L. Corradi, S. Courtin, D. Bourgin, E. Fioretto, A. Goasduff, J. Grebosz, F. Haas, M. Mazzocco *et al.*, *Phys. Rev. C* **92**, 064607 (2015).
- [52] C. L. Jiang, B. B. Back, H. Esbensen, J. P. Greene, R. V. F. Janssens, D. J. Henderson, H. Y. Lee, C. L. Lister, M. Notani, R. C. Pardo *et al.*, *Phys. Rev. C* **78**, 017601 (2008).